ORIGINAL RESEARCH

Lanthanides-Substituted Hydroxyapatite/*Aloe vera* Composite Coated Titanium Plate for Bone Tissue Regeneration

Selvakani Prabakaran[1]
Mariappan Rajan 🅰[1]
Changwei Lv[2]
Guolin Meng[3]

[1]Biomaterials in Medicinal Chemistry Laboratory, Department of Natural Products Chemistry, School of Chemistry, Madurai Kamaraj University, Madurai 625021, India; [2]Department of Orthopaedics, The Affiliated Hospital of Northwest University, Xi'an No.3 Hospital, Xi'an 710018, Mainland China; [3]Orthopaedic Department of Xijing Hospital of the Fourth Military Medical University, Xi'an, Shaanxi, 710032, Mainland China

Purpose: To develop the surface-treated metal implant with highly encouraged positive properties, including high anti-corrosiveness, bio-activeness and bio-compatibleness for orthopedic applications.

Methods: In this work, the surface of commercially pure titanium (Ti) metal was treated with bio-compatible polydopamine (PD) by merely immersing the Ti plate in PD solution. The composite of trivalent lanthanide minerals (La^{3+}, Ce^{3+} and Gd^{3+})-substituted hydroxyapatite (MHAP) with *Aloe vera* (AV) gel was prepared and coated on the PD-Ti plate by electrophoretic deposition (EPD) method. The choice of trivalent lanthanide ions is based on their bio-compatible nature and bone-seeking properties. The formation of the PD layer, composites, and composite coatings on Ti plate and PD-Ti surface was confirmed by FT-IR, XRD, SEM and HR-TEM observations. In-vitro assessments such as osteoblasts like MG-63 cell viability, alkaline phosphatase activity and mineralization ability of the MHAP/AV composite were tested and the composite-coated plate was implanted into a rat bone defect model for in-vivo bone regeneration studies.

Results: The coating ability of the MHAP/AV composite was highly preferred to PD-treated Ti plate than an untreated Ti plate due to the metal absorption ability of PD. This was confirmed by SEM analysis. The in-vitro and in-vivo studies show the better osteogenic ability of MHAP/AV composite at 14th day and 4th week of an experimental period, respectively.

Conclusion: The osteoblast ability of the fabricated device without producing any adverse effect in the rat model recommends that the fabricated device would serve as a better platform on the hard tissue regeneration for load-bearing applications of orthopedics.

Keywords: bio-compatible, electrophoretic deposition, hydroxyapatite, mussel adhesive protein, polydopamine, surface treatment

Introduction

The maturity growth of an implant device is an imperative need for return backs the patients from orthopedic diseases to a normal lifestyle with the increasing of life-quality.[1] The surface of the metal implants has played a vital role in the success rate of biologically active implants, which can be predicted by its ability of osseointegration from the strong interface interaction between bone tissues to implant material.[2] For improving the bio-activity, osseointegration and anti-corrosive properties of an implant material, various surface treatment techniques such as Micro-Arc oxidation,[3,4] Plasma spraying,[5,6] Ion implantation,[7,8] Laser surface

Correspondence: Changwei Lv
Department of Orthopaedics,
The Affiliated Hospital of Northwest University, Xi'an No.3 Hospital, Xi'an 710018, Mainland China
Email lucwei76@sina.com

modification,[9,10] and Friction stir processing[11,12] were applied on the surface of the bio-compatible Ti implants.

Mussel adhesive proteins (MAPs) have great interest due to their capability of allowing the mussels that adhered to a surface of different materials in wet conditions by *Mytilus edulis* foot protein (Mefp).[13] The primary substance 3, 4-dihydroxyphenylalanine (DOPA) is believed to the responsible for an adhesion property of MAPs.[14,15] The compound dopamine, having a similar chemical structure of DOPA, has been used as a novel material for the coating process.[16,17] The polydopamine (PD) – a biocompatible polymer – coating on the surface of the material can be easily formed via the dopaquinone (DQ), which is the oxidative product of dopamine under aerobic condition. The dopaquinone can easily convert into PD without the need for any specific reaction conditions.[18] The PD coatings can efficiently adsorb metal ions due to the presence of different functional groups like catechol, imine, and amine its unique structure.[19] In 2017, Wang et al have reported the bone marrow mesenchymal stem cells (BMSCs) binding factor displayed better cell adhesion, proliferation, and also differentiation on Bone Morphogenetic Protein-2 (BMP-2) loaded PD/HA composite-coated Ti plate.[20] From their report, it was believed that BMP-2 attachment and its controlled release might be due to the interaction between PD and growth factors. So, it is clear that the PD coating on Ti orthopedic implant will enhance the osseointegration of the Ti into implant. In addition, PD coating is also using in the organ-on-a-chip (OOC) systems that were developed by Khetani et al, 2020. The system is based on a flow-based coating technique to create reliable, reproducible, and ready-to-use microfluidic cell culture chips for OOC studies.[21] Moreover, in another study, they developed simple and cost-effective method by which it can be achieved the photo-activated polymerization of monomers such as dopamine and norepinephrine by exposure to UV light for the same OOC applications.[22] Besides, the high sintering temperature of the polymer may lead to the degradation of those polymeric materials. The alternate approach, in this way, will keep the polymers (PD) within the surface of the biomedical implant.

Moreover, one of the ancient medicinal plants which are frequently used in biomedical, cosmetics, and pharmaceutical applications is *Aloe vera* (AV), which belongs to the Liliaceae family.[23–25] The various medicinal properties such as anti-oxidant, anti-bacterial, anti-septic, anti-fungal, wound healing, anti-viral, anti-inflammatory and tissue

regeneration ability of AV plant have been reported in various studies.[23–28] An existence of these properties originated from the 75 biologically active compounds including amino acids, vitamins, polysaccharides, enzymes and various minerals that are presented in AV.[29]

In 2013, Jithendra et al have been reported the import of AV in fish collagen (COL)/chitosan (CS) composite has enhanced the thermal stability and hydrophilicity of the scaffold materials for tissue engineering.[30] The scaffold containing AV (COL-CS-AV) had enhanced the proliferation and growth rate on fibroblast 3T3L1 cell without produce any toxic effect when compared with fish collagen (COL)-chitosan (CS) composite.[30] In the very next year, Suganya et al, 2014 had fabricated the poly (lactic acid-co-caprolactone) (PLACL) electrospun fibers incorporated with AV, Silk fibroin (SF) and HAP for the enhancement of osteogenesis. The scaffold (PLACL-AV-SF-HA (4%)) had significant observation by increasing the cell proliferation, osteogenic differentiation, osteocalcin expression, and mineral deposition in comparison with different controls due to the osteoinductive and osteoconductive properties of AV and HAP, respectively.[31] The surface-coated Ti implant with natural AV gel extract, acemannan incorporated Ag and Si-doped HAP was investigated by Banerjee and Bose, in 2019 and was concluded that the natural AV incorporated Ag, Si-HAP containing implant could act as better bio-material for hard tissue regeneration.[32]

Calcium analogs are known as the substitutes with the ability of substitution for the calcium ion in proteins and cell membranes. Among many elements, trivalent lanthanum ions have more or less similar ionic radii to that of calcium ion, so the replacement of calcium by these trivalent lanthanum ions is highly interested.[33] From this origin, we have decided to choose the lanthanide trivalent ions such as La^{3+}, Ce^{3+} and Gd^{3+} for the substitution of calcium in the hydroxyapatite (HAP) matrix. HAP is a well-known bio-ceramic material that has a major portion of the natural bone.[34,35] The recent report published by Lou et al suggests the bonding strength between the HAP and Ti surface and the cytocompatibility of the coating were enhanced with the addition of La^{3+} in HAP towards the proliferation and differentiation of MC3T3-E1 cells.[36] Owing to the anti-bacterial activity and non-toxic nature at the lower concentration for a longer time, trivalent cation Ce^{3+} possess the higher safety ion and the availability of various biological evidence, such as in-vitro studies for its prevention of initial bacterial adhesion property,[37,38] Ce^{3+} has chosen as an anti-bacterial mineral. In recent, Zhu et al had reported the addition of Gd in

bioactive glasses (BG) scaffold was exhibited superior bio-compatibility, osteoinductivity, and improved in a proliferation of human Bone Marrow derived Mesenchymal Stem Cells (hBMSCs). Moreover, the in-vivo results show that bone regeneration ability was higher for Gd doped BG than undoped BG.[39] For this reason, the trivalent lanthanide ion Gd^{3+} was added along with these minerals on the HAP matrix.

Encouraged by the bio-compatible and bio-active properties of these materials towards the hard tissue regeneration, La^{3+}, Ce^{3+} and Gd^{3+}-substituted HAP (MHAP) reinforced with AV gel for an electrophoretic Deposition (EPD) on PD-treated Ti metal plate was prepared. Our study presents overcome the limitations of previous investigations by the way of incorporating the lanthanide ions in HAP and composite coating on the PD surface-treated Ti implant. In fact, there are no other reports that deals with the coating of Ti implant by PD and Lanthanides doped HAP incorporated with natural AV. In this regard, the effect of lanthanide series elements (La^{3+}, Ce^{3+} and Gd^{3+})-substituted HAP, AV and PD coating on Ti metal to the growth and differentiation of bone cells in both in-vitro and in-vivo rat model was investigated. The schematic representation of this work is given in Figure 1.

Experimental Sections
Materials

For the preparation of bio-composites, the following chemicals were utilized and were purchased from commercial sources. Calcium chloride dihydrate ($CaCl_2.2H_2O$), Cerous chloride heptahydrate ($CeCl_3.7H_2O$), Lanthanum chloride heptahydrate ($LaCl_3.7H_2O$), Gadolinium chloride hexahydrate ($GdCl_3.6H_2O$), diammonium hydrogen phosphate

((NH_4)$_2HPO_4$), ammonium hydroxide (NH_4OH), 2-propanol as the solvent for EPD, Dopamine hydrochloride, ethanol and the Ti metal plate (commercially pure Ti, 99.7%) for the coating of the prepared composite were purchased from Sigma-Aldrich, India. The fresh leaf of AV was obtained from the water-rich area in Madurai (9.7354° N, 77.7896° E), Tamilnadu. All the reagents/chemicals were used as such as received, and there was not mandatory for further purification. Double-distilled (DD) water was used throughout the experiment for washing and reactions.

Preparation of AV Gel Solution

AV leaf was collected from the water-rich area in Madurai (9.7354° N, 77.7896° E), Tamilnadu. Selectively the matured leaf with proper growth (3 cm in length) was collected. The leaf was then washed with water and ethanol. AV gel solution was prepared by separating the gel from the AV leaf by scratching the inner part of the leaf. After collecting the gel, about 5g of the gel was weighed and dissolved in 25 mL of water. This solution was used for the source solution of AV for further reactions.

In-situ Preparation of AV Incorporated Lanthanides-Substituted HAP Materials

At first, the raw solutions of the cationic minerals La, Ce, Gd and Ca were prepared by dissolving the corresponding mineral salts such as $LaCl_3.7H_2O$, $CeCl_3.7H_2O$, $GdCl_3.6H_2O$ and $CaCl_2.2H_2O$ in DD water, separately. The solution containing phosphate (P) anion was prepared by dissolving the phosphate salt ((NH_4)$_2HPO_4$) in DD water in a separate beaker. The molar ratio of minerals was maintained as 1.67 by taking La, Ce, Gd & Ca/P solutions as the molar ratio of
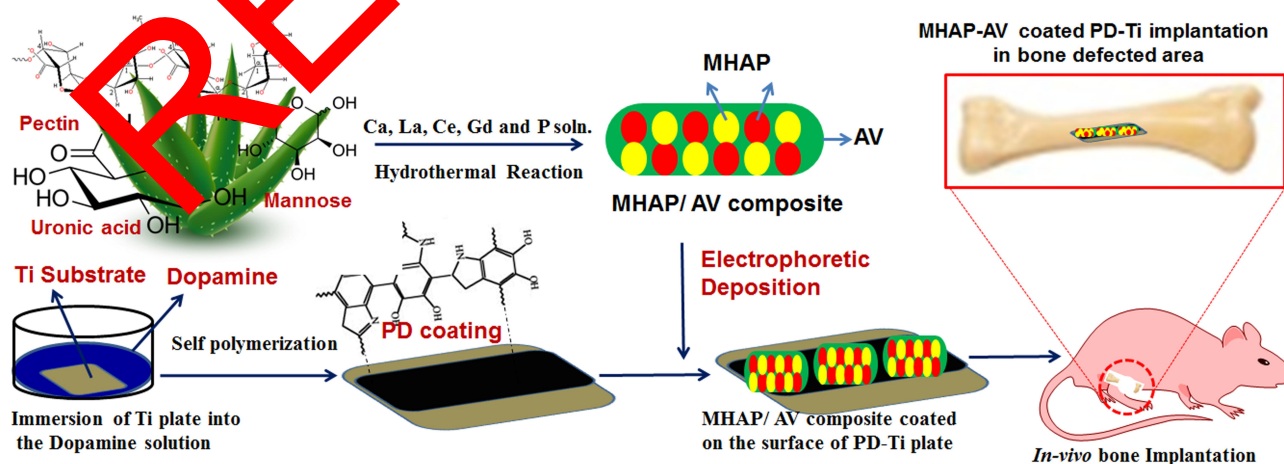

Figure 1 Schematic representation of the present study.

0.05+0.05+0.05+0.35/0.335 mole, respectively. Initially, the La, Ce and Gd solutions were mixed slowly with the Ca solution by utilizing the burette and allowed stirring in magnetic stirrer for 1 h to ensure the effective interaction between the ions. Then the mineral solution was added slowly into the prepared AV gel solution under the vigorous magnetic stirring. The pH of the solution was adjusted to 11.0 by using NH_4OH and maintained throughout the reaction. Further, the phosphate solution was added slowly in a drop wise manner into the mixture solution of minerals and AV gel for 3–4 h under vigorous magnetic stirring with the formation of slight brown precipitates. All the steps involved in the above procedure were carried out at room temperature (27 ºC). After stirring for 12 h, the resultant mixture was subjected to ultrasonic irradiation (Ultrasonics model with 130 W supply and 5 sec on, 2 sec off time) at 28 kHz for 10 min to achieve the mutual interaction between AV and MHAP. Then, it was transferred to a Teflon vessel and treated at the temperature of 90 ºC in an autoclave for 24 h. Finally, the sol was filtered and the powders were washed with water and ethanol. The obtained powder was then dried at 75 ºC in hot air oven to get the dried AV incorporated MHAP composite.

The PD Coating on Surface-Treated Ti Plate

Before the utilization of commercially pure Titanium (Ti) plate (10 × 10 × 0.3 mm in size), the surface was polished mechanically with the silicon carbide paper with 400–1500 grades and treated with an acid solution of H_2SO_4/H_3PO_4 (7/3 of mixture ratio). Further, it was washed ultrasonically with water, ethanol and acetone for 30 min by each of the solvent at room temperature (27 ºC). The PD coating on the surface-treated Ti plate was carried out by an immersion of the sample in PD solution for 24 h at 27 ºC. The PD solution was prepared by dissolving 20 mg of dopamine hydrochloride in 10 mL of Tris buffer (10mM, pH 8.5) at 27 ºC. The dopamine hydrochloride was polymerized into PD by atmospheric oxygen, and the black layer was formed on the Ti surface. Then the PD-coated Ti (PD-Ti) plate was washed with water and ethanol to remove the uncoated particles and then dried at 60 ºC for 5 h.[40]

Electrophoretic Deposition (EPD) of Composite on Ti Plate

The MHAP/AV composite was dispersed in 2-propanol for making an electrolyte solution for depositions. The PD-Ti

plate was acted as a working electrode (cathode) and the flag shape platinum electrode was used as a reference electrode (anode). The distance between these two electrodes is set as 1 cm, and the constant voltage of 30 V for 20 min was applied at room temperature (27 ºC) for an even and efficient coating of the composite.

Phase, Functional and Morphological Characterizations
XRD Analysis

The diffractometer system (XPERT PRO) was used for identification of phase and the crystallinity of all prepared composites with Cu K_α incident radiation over the 2θ range of 10º to 80º, worked at 40 kV and 30 mA and scanning rate (2θ) of 0.2º.

FT-IR Analysis

All of the prepared composites and individual components were confirmed by their functional group analysis. This was done with IRTRACER-100 Infra-Red absorption spectroscopy (Shimadzu) using the KBr pellet method. In the region of wave-numbers from 4000 cm^{-1}–400 cm^{-1}, the spectra were recorded at 4 cm^{-1} resolution.

SEM and HR-TEM Analysis

The morphology of the prepared composites and the minerals that are present in those composites were evaluated by scanning electron microscopy (SEM) combined with energy-dispersive X-ray spectroscopy (EDX) (JEOL JSM-6400, Japan). The SEM morphology was detected after coating the water dispersed composites on a glass plate.

The model of JEOL JEM 2100 Co., Tokyo, Japan, High-resolution transmission electron microscopy (HR-TEM) was utilized for evaluating the microstructure of all prepared composites. Selected area electron diffraction (SAED) was also performed in order to identify the constituent phases. The HR-TEM was carried out after coating the water dispersed composites on a gold grid.

Zeta Potential

The zeta potential method was utilized for evaluating the charge of the surface of the composites by using the Delsa analyzer instrument (Beckman colter) with water as dispersant at 25 ºC.

Vickers Micro-Hardness (Hv) Test

The withstanding ability of the metal implants determines the success of that implant during in-vivo implantation

under load-bearing applications. The most important property to evaluate the mechanical performance of the metal implant is a Vickers micro-hardness test. The surface-treated Ti plate with different coating conditions was subjected to a micro-hardness test with a Vickers pyramid indenter by using an Akashi AAV-500 series hardness tester. The load and dwell time was set as 490 mN and 20 s, respectively. The obtained value of Hv (Vickers pyramid number) was averaged with the three repeated experiments.

Bio-Activity of the Immersed MHAP/AV Composite Coated on PD-Ti Plate in Simulated Body Fluid (SBF)

The SBF solution with the same ionic concentration of human blood plasma was prepared by the procedure reported by Kokubo et al.[41] After the preparation of the SBF solution, and the surface-treated MHAP/AV bio-composite-coated Ti implant was immersed in the solution at 27 ºC for 1, 3, and 7 days in a sealed bottle to assess the bio-activity and bone-bonding ability of implant material. Then the implant was taken away from the SBF solution after the completion of a specific period and then washed with DD water, dried and examined by SEM and XRD analysis.

Bone Regeneration Ability Studies
In-vitro Cell Growth

MG-63 osteoblasts-like cells were obtained from National Center for Cell Science (NCCS, Pune, India). The normal culture medium of Dulbecco's Modified Eagle Medium (DMEM, GIBCO) with animal essential media (Hi-Media Laboratories) was utilized to maintain the cells in 24-well tissue culture plates with the supplementation of 10% Fetal Bovine Serum (FBS), penicillin (100 U mL^{-1}) and streptomycin (100 U mL^{-1}) for 4 h. After that, the normal media was replaced by introducing fresh growth media. Then the growth circumstance was changed to the humidified atmosphere of 95% air and 5% CO_2 at 37 ºC. To remove the unwanted moieties in the composite sample specimens for examinations, they were sterilized at 90 ºC for 120 to 150 min in an autoclave and then placed in 96-well cell plates.

In order to evaluate the cell attachment and proliferation quantitatively, MTT assay was performed by measuring the mitochondrial dehydrogenase activity. The MG-63 osteoblasts-like cells loaded medium was detached from the culture after 1, 3, 7, and 14 days and shifted into new 96-well cell plates with the density of 1×10^4 cells per well to assess

the cell proliferation. After 24 h, 2 mL of MTT (3-(4,5-dimethyl-2-thiazolyl)-2,5-diphenyl-2H-tetrazolium bromide) solution in serum-free medium was added to every sample and then incubated under a humidified atmosphere containing 5% CO_2 for 4h at 37 ºC. The solution was removed, and to dissolve the formazan crystals, 10% DMSO was added to every well plates for 15 min. The cell proliferation speed was assessed by observing the optical density (OD) values at 570 nm on the spectrophotometric microplate, and the following equation calculated the percentage of cell viability. This experiment was averaged by 3 replicates.[42]

$$\% \, cell \, viability \, = \, [A]_{test}/[A]_{control} \times 100 \qquad (1)$$

Alkaline Phosphatase (ALP) Activity

After 1, 3, 7, and 14 days of culture, the intracellular ALP activity of the MG-63 osteoblasts-like cells on samples was assessed by the substrate hydrolysis of β-nitrophenyl phosphate. Simply, the cells after a particular time were lysed in 0.1% Triton X-100 by freeze-thaw rotations at 4 ºC for 1 h after the washings with Dulbecco's phosphate-buffered saline (D-PBS) for three times. The microplate reader was used to predict the absorbance of the product amount of p-NPP measured at the OD value of 405 nm.[42]

Determination of Calcium Deposition on MG-63 Osteoblasts Cells by Alizarin Red S (ARS) Staining

The mineralization of calcium on MG-63 osteoblast cells after 1, 3, 7 and 14 days of incubation with tested samples was determined by ARS staining. After the completion of specific time periods, the cells were fixed with ethanol (95%) for 1 h and then washed with DD water. The staining was carried out by immersion of samples in 2% of Alizarin red S solution for 10 min at 27 ºC and then several times washed with DD water before taking image under a bright field microscope. For quantification of deposition, 10% of cetylpyridinium chloride (CPC) was used to dissolve the Alizarin red for the disappearance of red color. After 1 h of incubation, the absorbance was measured at OD value of 405 nm.[43,44]

In-vivo Animal Studies
Implantation Procedure

The protocols for the animal experiments were followed according to the guidelines of the Institutional Animal

Ethics Committee (IAEC) at Kovai Medical Center Research and Educational Trust, Coimbatore, India, and Biosafety and Animal welfare committee. And this study performing with animals was approved by the Institutional Animal Ethics Committee (IAEC) at Kovai Medical Center Research and Educational Trust, Coimbatore, India. The bone healing and regeneration ability of lanthanides substituted HAP encompassing with AV composite coated on the PD-Ti implant was assessed bythe rat surgical model analysis. From the in-vitro studies, we confirmed the bio-activity and bio-compatibility of the composite materials and further; this was moved to animal studies. 6-month-old Wistar male rats (n=6) with an average body weight of 200–250 g were selected, and the hole with the critical size (2 mm) was created by using the supreme micro motor at the disinfectant site. To remove the heat effect during implantation, the constant irrigation of PBS was carried out followed by an implantation. All rats were housed at 22 ± 2 ºC before implantation, and the alternating 12 h light/12 h dark cycle was maintained in a room for 2 weeks to accommodate the proper diet and clean water. Initially, the rats were prepared for surgery by removing the hair by shaving in the operation site. Then the defect was created at the leg on the left side and scrubbed with 10% providing-iodine for skin disinfection. The ketamine and xylazine were injected about 20 mg/kg and 2 mg/kg, respectively, through an intraperitoneal injection followed by the inhalation of 20% isoflurane and propylene glycol mixture which was used to anesthetize all rats individually. After the operation, all rats were given penicillin for 1 week to prevent bacterial infection and kept under observation to notice their free movement.[45]

X-Ray Analysis and Histopathological Assessment

After the scarification of the rat at 1st, 2nd, 3rd and 4th weeks of implantation, the new bone formation was imaged using soft X-ray, and the implant bones were cut and fixed in 20% of neutral formalin solution followed by the bones were decalcified with 10% solution of the acetic acid at 4 ºC for 2 weeks with the replacement of solution for every 2 days and inserted in paraffin. The section with the thickness of 4 μm was stained with Hematoxylin and Eosin (HE) solution and Masson's trichrome staining (MTS) and noted under light microscopy.

Statistical Analysis

All experiments were conducted in triplicate and expressed as ± standard deviation for the as-developed composite coatings. Analysis of variance (ANOVA) with Tukey's multiple comparison tests (Prism, version 5.0) was used to perform the statistical analysis, and p<0.05 was considered to be statistically significant for the difference observed between the groups.

Results and Discussion
Functional Group Analysis

Figure 2 shows the functionality that presents in all prepared compounds such as HAP, MHAP, HAP/AV and MHAP/AV composite, which were evaluated by FT-IR spectroscopy (Figure 2A and B). The FT-IR spectrum given in Figure 2a corresponds to the functional groups of pure HAP ceramic and evidencing the formation of HAP ceramic. The peaks are mainly arising due to the presence of phosphate (PO_4^{3-}) group in HAP lattice. The modes of fundamental vibrations appeared at 1111.63 cm^{-1} and 1026.84 cm^{-1} (v_3), 472.63 cm^{-1} (v_2), 635.20 cm^{-1} (v_4) and 955.0 cm^{-1} (v_1) for the PO_4^{3-} group in pure HAP. Moreover, the sharp absorption peak appears at 568.9 cm^{-1} for the vibration mode of the hydroxyl group (-OH) of the HAP.[46] The La, Ce, and Gd minerals substituted on the HAP lattice, which is replacing the Ca^{2+} ions, were affecting the intensity of PO_4^{3-} absorption peak in Figure 2Ab. This FT-IR spectrum had clearly showed that an intensity of v_2 absorption peak and an absorption peak of -OH vibrational mode was decreased due to the breakage of the electric charge balance in the HAP lattice caused by the substitution of divalent Ca^{2+} ion with trivalent lanthanide (Ln^{3+}) ions. But the position of PO_4^{3-} absorption peaks was retained as placed in pure HAP spectrum.[47] The identification of Gd^{3+} ion in FT-IR spectrum is difficult due to the smaller ionic radii of Gd^{3+} (1.00 Å) ion than the Ca^{2+} (1.04 Å) ion. So the Gd^{3+} ion neither appears in FT-IR result nor influence the spectral parameter of HAP lattice.[48] The influence of AV gel in HAP and MHAP ceramic's functionality is showed in Figure 2Ac and (d). In both the spectra, there appeared the broad absorption band in the -OH region. The broad band was centered at 3438.68 cm^{-1}, which exhibits the intermolecular hydrogen bonding stretching frequency of -OH groups in the monomers of carbohydrates, particularly mannose and uronic acid.[49] The absorption peaks at 1633.15 cm^{-1} and 1423.94 cm^{-1} correspond to the asymmetrical and
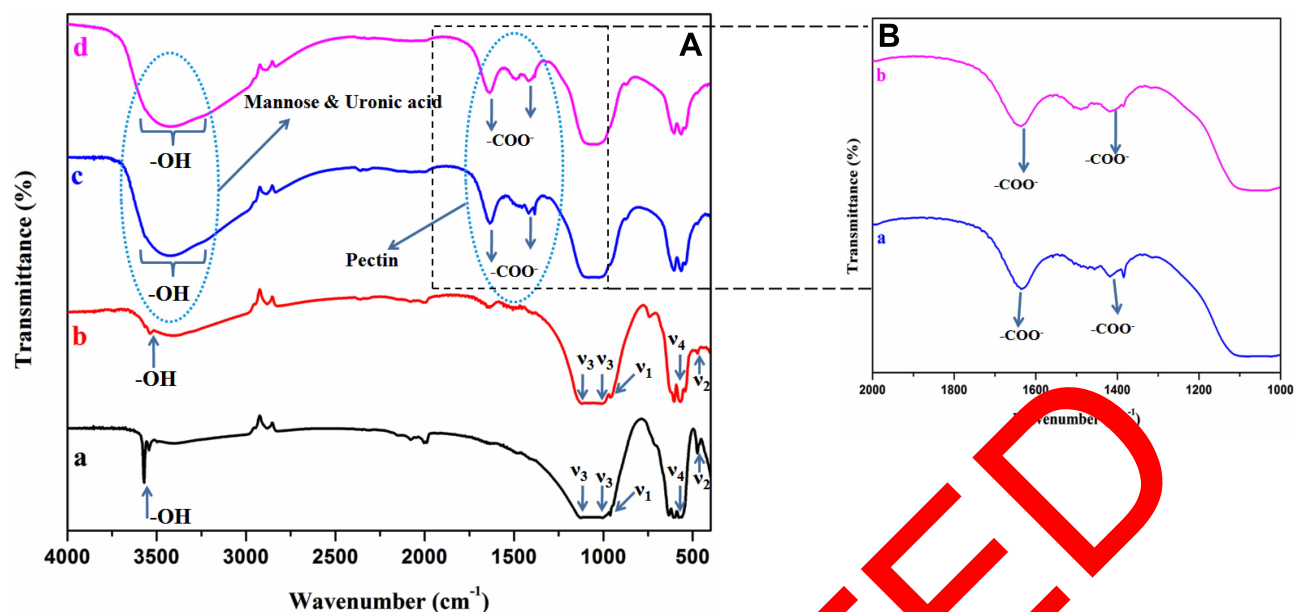
Figure 2 (**A**) FT-IR spectra of (a) HAP, (b) MHAP, (c) HAP/AV composite and (d) MHAP/AV composite. (**B**) Indication of pectin absorption peaks for the composites (a) HAP/AV and (b) MHAP/AV composite at the range of 2000–1000 cm^{-1}.

symmetrical stretching frequency of carboxylate (-COO$^-$) compounds, which characteristics of pectin molecule from AV gel.[50] Even with the substitution of minerals in HAP/AV composites, the structure was not distorted, and is evident from Figure 2Ad. The both -OH band and pectin peaks are not varied hugely. However, its intensity was slightly decreased as the negligible manner. In Figure 2Ba and b, the pectin absorption peaks for the composites are separately shown in the region of 2000–1000 cm^{-1}, which is evidence for the stability of HAP/AV composite even after the substitution of lanthanide minerals (La, Ce, and Gd).

Phase Analysis

The phase analysis of synthesized HAP, MHAP, HAP/AV and MHAP/AV composites was investigated by the XRD techniques and the results are present in Figure 3. The formation of HAP with higher crystalline nature was evidenced from the XRD pattern, as showed in Figure 3A. The sharp peaks present at 2θ values of 26.1º, 28.2º, 31.9º, 33.2º, 34.4º, and 40.1º were attributed to the HAP (002), (210), (211), (300), (202) and (212) planes, respectively.[51] The pure HAP phase diffractograms were showed with its JCPDS card number 9–0432. A slight undergoing deviation in positions of planes and the decrease in crystalline nature were observed when the lanthanide trivalent cations were substituted on the Ca^{2+} ion's matrix. This substitution was affected by the crystalline nature of the HAP, as

showed in Figure 3B. Moreover, some peaks in the planes of (300), (202), (212) and (222) were disappeared, and the intensity of existing peaks is also decreased and broadened during the AV substitution in both the HAP and MHAP ceramics as showed in Figure 3C and D. This clearly showed that the crystallinity of the compound is being changed with the entering of external organic moiety into the apatite lattice.

Besides, the crystallites size of all compounds was calculated by using Debye-Scherrer's equation by determining full width at half maximum (FWHM) value of all peaks that corresponding to the particular planes. By this calculation, the average crystallite size of pure HAP was found in the range of ~5.2 nm. In the case of the MHAP particle, the average crystallite size was calculated as around ~4.1 nm. From this crystallite size, it has been evaluated that the lanthanide trivalent ions were influenced by the crystal growth of HAP rods. In the case of AV substitution, a great difference has been observed between the crystallite sizes of MHAP and MHAP/AV. The average crystallite size of MHAP/AV was found as ~6.2 nm. This result has suggested that the introduction of AV into MHAP had produced the lattice strains on the MHAP matrix with dislocation of MHAP crystal. The high aspect ratio of the MHAP/AV compound may occur due to the growth of HAP crystals on the surface of AV that contains large biomolecules with pectin, mannose, uronic acid, etc.[52] These biomolecules can form a long chain with
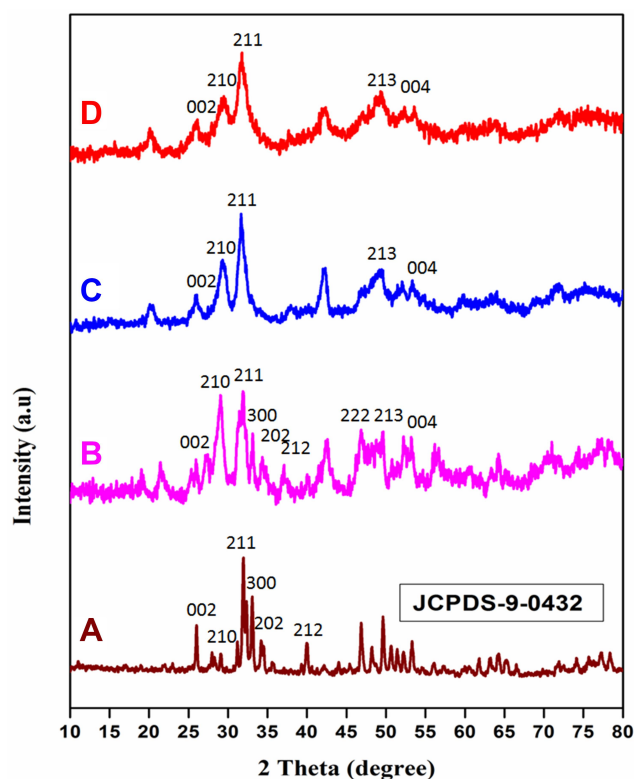
Figure 3 XRD patterns of (**A**) HAP, (**B**) MHAP, (**C**) HAP/AV composite and (**D**) MHAP/AV composite.

other hydrophobic and hydrophilic entities that present in water. After the AV had mixed with the cerium and lanthanide mixture solution, the lone pair electron of O^- or other negatively charged ions of AV will easily attract the divalent Ca^{2+} and trivalent lanthanide ions. In final, the formation and growth of HAP crystal on the long chain AV had occurred when the addition of phosphate solution in the AV and cations containing solution.

Morphological Observation by SEM Technique

The micro-structural evaluation of the composites HAP, MHAP, acid-etched Ti, PD-Ti, MHAP/AV, MHAP/AV coated on Ti (without treated with PD), and MHAP/AV coated on PD-treated Ti plate was carried out, and the results are given in Figure 4. The SEM morphological similarities were observed on the compounds of HAP, MHAP and MHAP/AV composite, as shown in Figure 4A and B and E. By the influence of hydrothermal treatment, the HAP crystal has exhibit rod-like morphology under pressure created by the hydrothermal reaction with a different temperature than the physiological temperature of the samples.[53,54] Figure 4C and

D and G are depicted the surface morphology of acid-etched Ti plate after sintering at 400 ºC, PD-treated Ti surface, and MHAP/AV-coated PD-Ti, respectively. A cross-section image of the coating of composite on the PD-treated Ti plate is given in Figure 4H. The PD was deposited evenly on the Ti surface, as evidenced from Figure 4D. In further, the MHAP/AV composite coated on PD-treated Ti as denser and compact with a thickness of ~15 μm, and the composite has fully covered the surface of PD-treated Ti plate as the results from EPD method. Figure 4F represents the morphology of MHAP/AV coated on the Ti plate (absence of PD treatment). It indicates the coating was not in compact manner, and the composite did not fully cover the surface of the Ti plate. This is well correlating with our previous report.[46] In also that previous study, the MHAP/PSSG composite was coated on the Ti plate with a loosely bound manner and as compared with the SEM image of MHAP/AV coated on the Ti plate (absence of PD treatment) in Figure 4F, herein MHAP/AV composite was coated with a compact network on the PD-Ti plate. This may occur due to the presence of PD on the surface of the Ti plate, which attracts more amounts of MHAP particles than an untreated Ti plate. The elements that present in the prepared composite were showed in EDX spectra is given in Figure 5. From this EDX analysis, it was confirmed that the substituted minerals (La, Ce, and Gd) were presented along with the Ca, P, and C elements, and the MHAP was formed with the atomic ratio of 1.69. The obtained atomic % of each element from EDX analysis is given as follows: C (AV)=33.49%, Ca=27.39%, P=25.82%, La=3.39%, Ce=3.35% and Gd=3.53%.

Morphology Analysis by HR-TEM Analysis

In continuation of SEM analysis, the micro-structures of the HAP, HAP/AV, MHAP and MHAP/AV composites were further evaluated from HR-TEM analysis. It reveals that the rod-like morphology of all prepared composites was observed by the hydrothermal reaction (Figure 6A–D). By the ImageJ software analysis, the substitution of AV in the MHAP matrix does not affect the diameter of nano-rods. The average width of the nano-rods was found as ~6.9 and ~6.1 nm for MHAP and MHAP/AV composite, respectively. The length of HAP nano-rods was affected by the influence of AV incorporation in the MHAP matrix. The length of MHAP nano-rods was calculated as ~38.38 nm, while
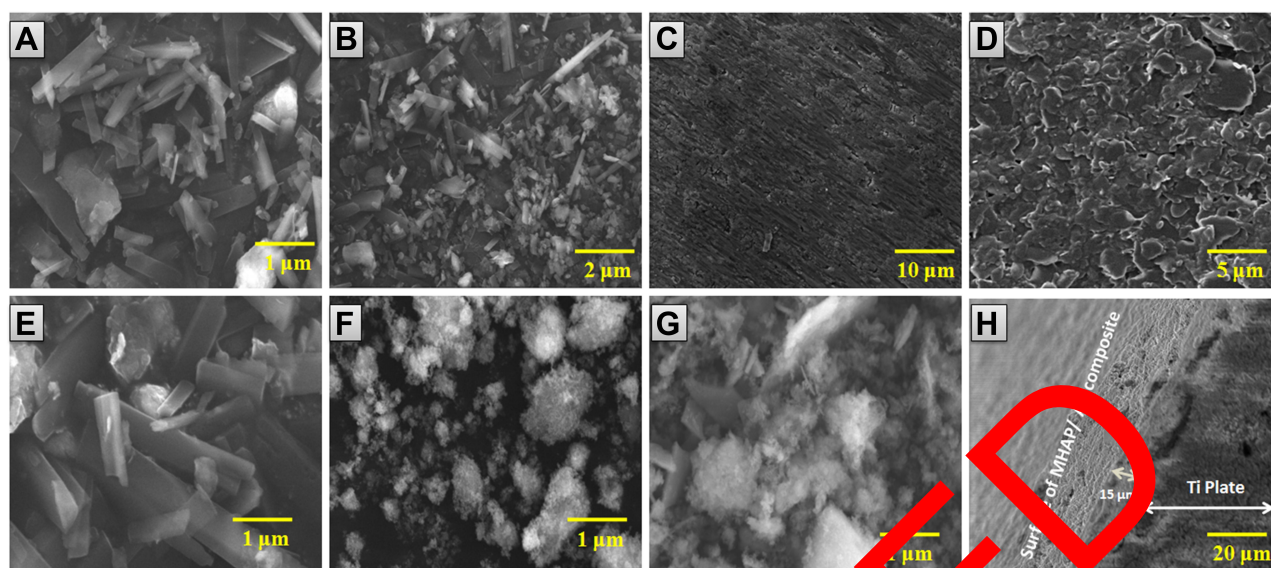
Figure 4 SEM morphology of (**A**) HAP, (**B**) MHAP, (**C**) Acid-etched surface of Ti plate after sintering at ___ °C for 5 __ (__) PD-tre___ Ti, (**E**) MHAP/AV, (**F**) MHAP/AV composite coated on Ti plate (Absence of PD treatment) (**G**) Surface of PD-Ti plate after coating wi__ __HAP/AV compo___ and (**H**) Cross-section image of MHAP/AV composite coated on PD-treated Ti plate.

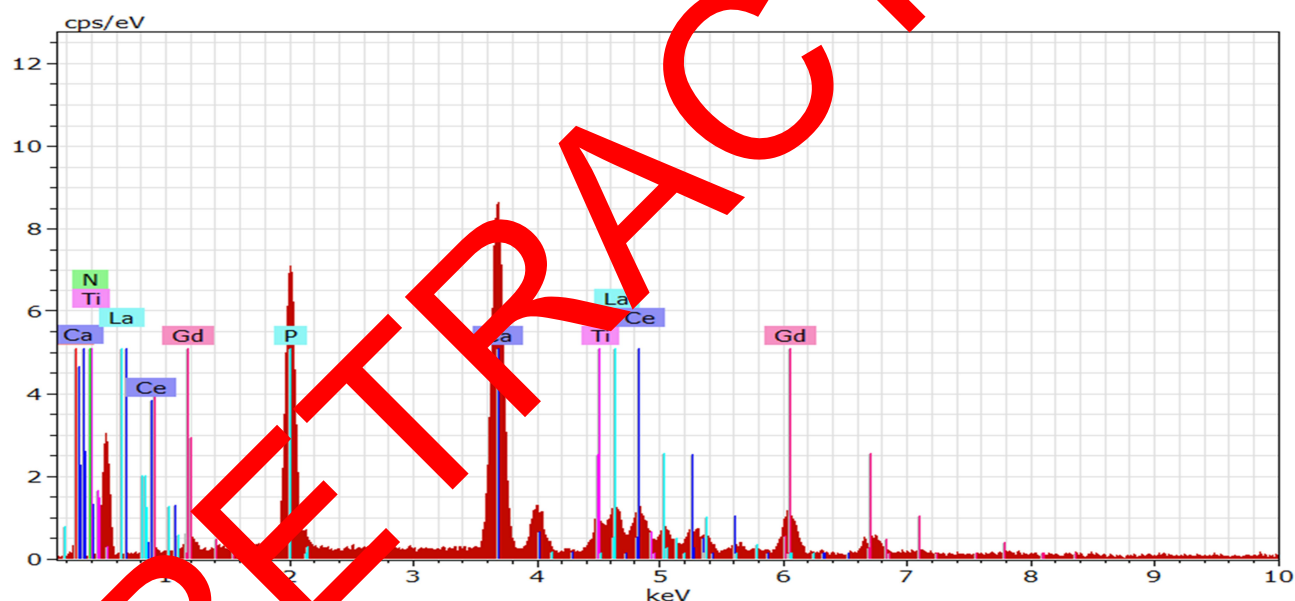**Figure 5** E__X spec___ __ __rmation of elements present in the MHAP/AV composite coated on PD-Ti plate.

in the AV-substituted composite, it was found as ~42.91 nm. This is another evidence for the lattice strains that were produced on the MHAP matrix by an influence of AV as supported to XRD results. This alteration of the length of the nano-rods after AV incorporation can serve as the confirmatory result for the fact that an adjustment of crystal growth of the MHAP matrix is made by AV components. Similarly, the length and diameter of the HAP were calculated as

~50.2 and ~7.5 nm. After the incorporation of AV in the HAP matrix, its length was increased up to ~65.3 nm, and the diameter becomes ~8.2 nm. The SAED pattern of the HAP, HAP/AV, MHAP and MHAP/AV composites is showed in insets of Figure 6A–D. The SAED results firmly stand for the above concept of the influence of AV in the crystallinity of the MHAP matrix. The distribution of diameter and length histogram charts is shown in Figure 7A–H.
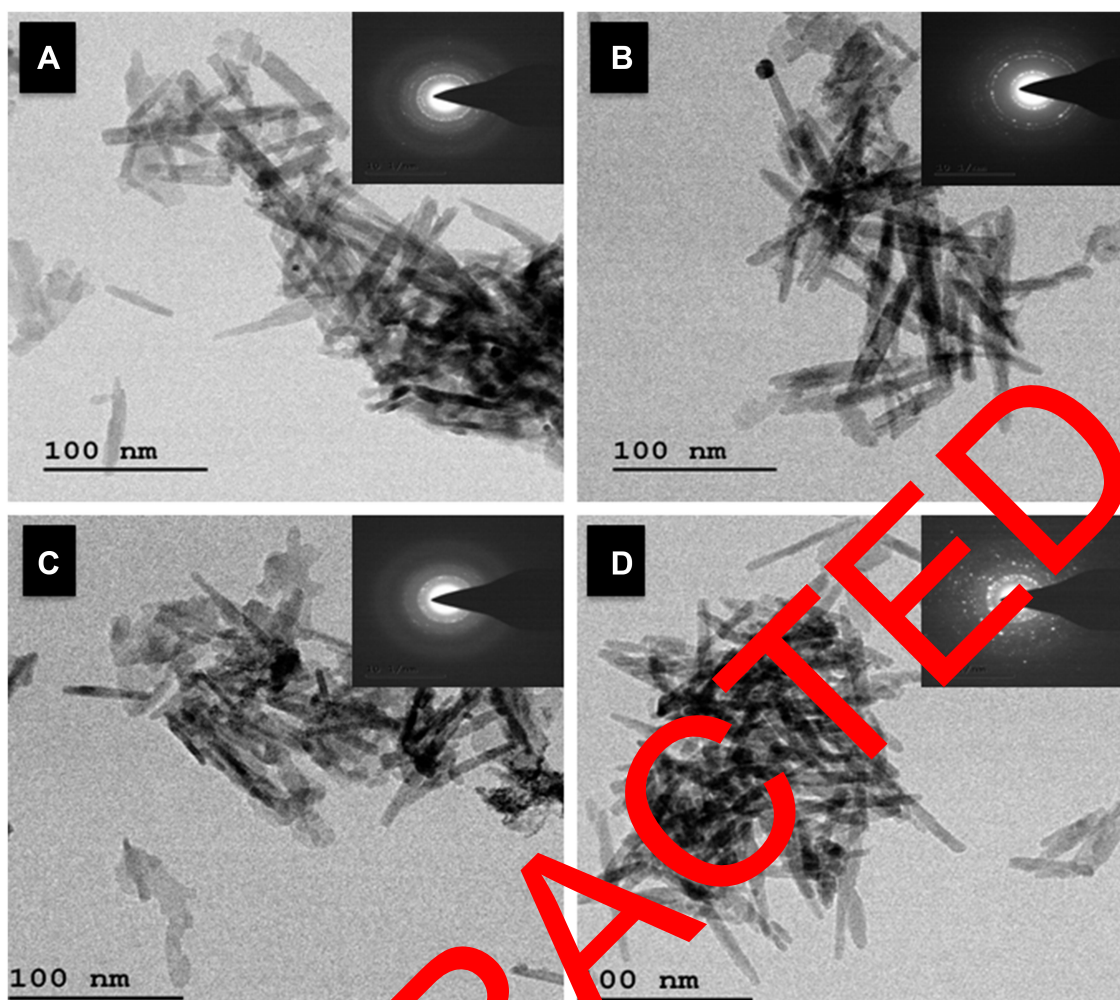
Figure 6 HR–TEM images of (**A**) HAP, (**B**) HAP/AV, (**C**) MHAP and (**D**) MHAP/AV nano rods and the SAED patterns of the all prepared compounds were given in insets of their corresponding TEM images.
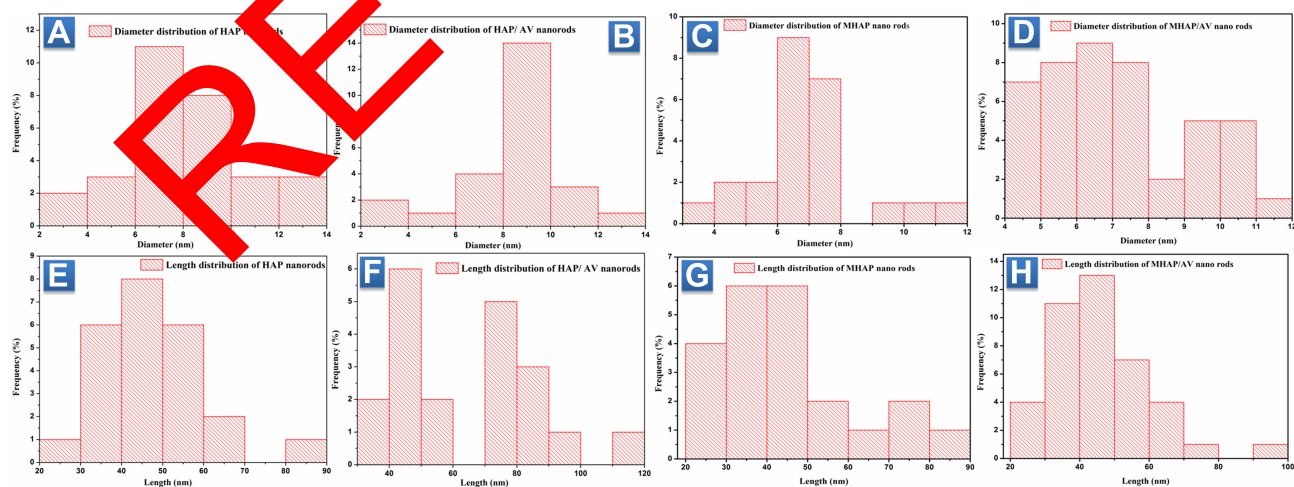

Figure 7 (**A–D**) Diameter distributions of HAP, HAP/AV, MHAP and MHAP/AV nano rods, respectively, (**E–H**) Length distributions of HAP, HAP/AV, MHAP and MHAP/AV nano rods, respectively.

Surface Charge Analysis for an Assessment of Bioactivity of the Composite

An alteration made by an influence of AV in MHAP/AV composite, in the physicochemical properties of the MHAP matrix will also alter the biological performance of the composite to favor the bone growth as faster than MHAP. The formation of apatite crystals on the surface of the composite-coated Ti plate is the best indicator of the bio-activity of the composite. The apatite crystal would form on the more negative charged surface than a less negative or positive charged surface.[55] The more electronegative charge containing surface is a favorable site for the growth of the apatite layer because initially, the absorption of Ca^{2+} ions is more preferential for that negatively charged surface. As a result of these Ca^{2+} ions, the negative charge will decrease and move towards the positive charge. Automatically, the absorption of phosphate ions would take place on the positively charged Ca^{2+} surface. Based on the mechanism, the apatite nucleation occurred on the more negatively charged surface of the material.

By measuring the zeta potential value in terms of surface charge of the composite, it will help to find out the bio-activity of the implants. The lower value of the zeta potential was observed for MHAP/AV composite when compared with the MHAP matrix. This increment in the value of zeta potential may have resulted from the AV incorporation in the MHAP/AV composite since AV has more negative functional groups, as discussed in the XRD section. The zeta potential values of MHAP and MHAP/AV are found as −15.07mV and −18.52mV, respectively. From the zeta potential results, we have confirmed that the MHAP/AV composite-coated Ti implant would serve as a better bio-active implant than HAP or HAP/AV or MHAP-coated Ti implant. The mobility distribution curve is given in Figure 8A and B.

In-vitro Apatite Formation of the Composite-Coated Implant in SBF Solution

The bone-bonding ability of the particular composite-coated Ti implant is the scale of predicting its bio-active nature when applying to in-vivo implantation. The formation of apatite crystals will act as the bridge between the implanted plate and the host bone tissue. The apatite will make the bio-active bond between the surface of implanted material and living bone tissue when implantation. It will help the osteointegration of the implant material for new bone formation. The MHAP/AV composite coated on the PD-Ti implant was soaked in SBF solution for 1, 3 and 7 days and analyzed their bone-bonding nature in terms of finding the apatite crystals formation. The morphology of the apatite formation was viewed by SEM analysis and given in Figure 9. As the period increases, the structure of apatite crystals is more on the MHAP/AV-coated PD-Ti implant. The original rod-like morphology was disappeared slowly when immersed in SBF for long days as a result of the formation of apatite crystals. Figure 9A–C indicates the formation of apatite crystals on the MHAP/AV composite-coated PD-Ti plate immersing in the SBF solution for 1, 3 and 7 days. After completion of 7 days of immersion, the apatite crystals were formed as a flake-like structure with small rod morphology. This result confirms the bioactive nature of the implant, and it is bio-compatible for further in-vivo implantation in terms of the formation of a bond between the implant and native bone of the body. Moreover, the formed apatite crystals were existed in weak crystalline nature evidenced from XRD diffraction pattern getting after immersion of MHAP/AV composite-coated PD-Ti plate in SBF solution (Figure 9D). After 1st day of immersion, the peaks in Figure 9Da were raised due to the apatite formation on MHAP/AV composite-coated PD-Ti surface. The weak
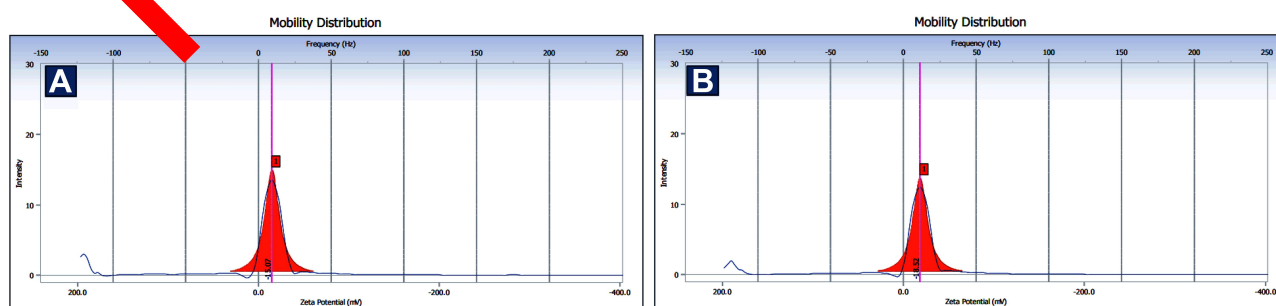

Figure 8 Zeta potential mobility distribution curve of (**A**) MHAP and (**B**) MHAP/AV composite.
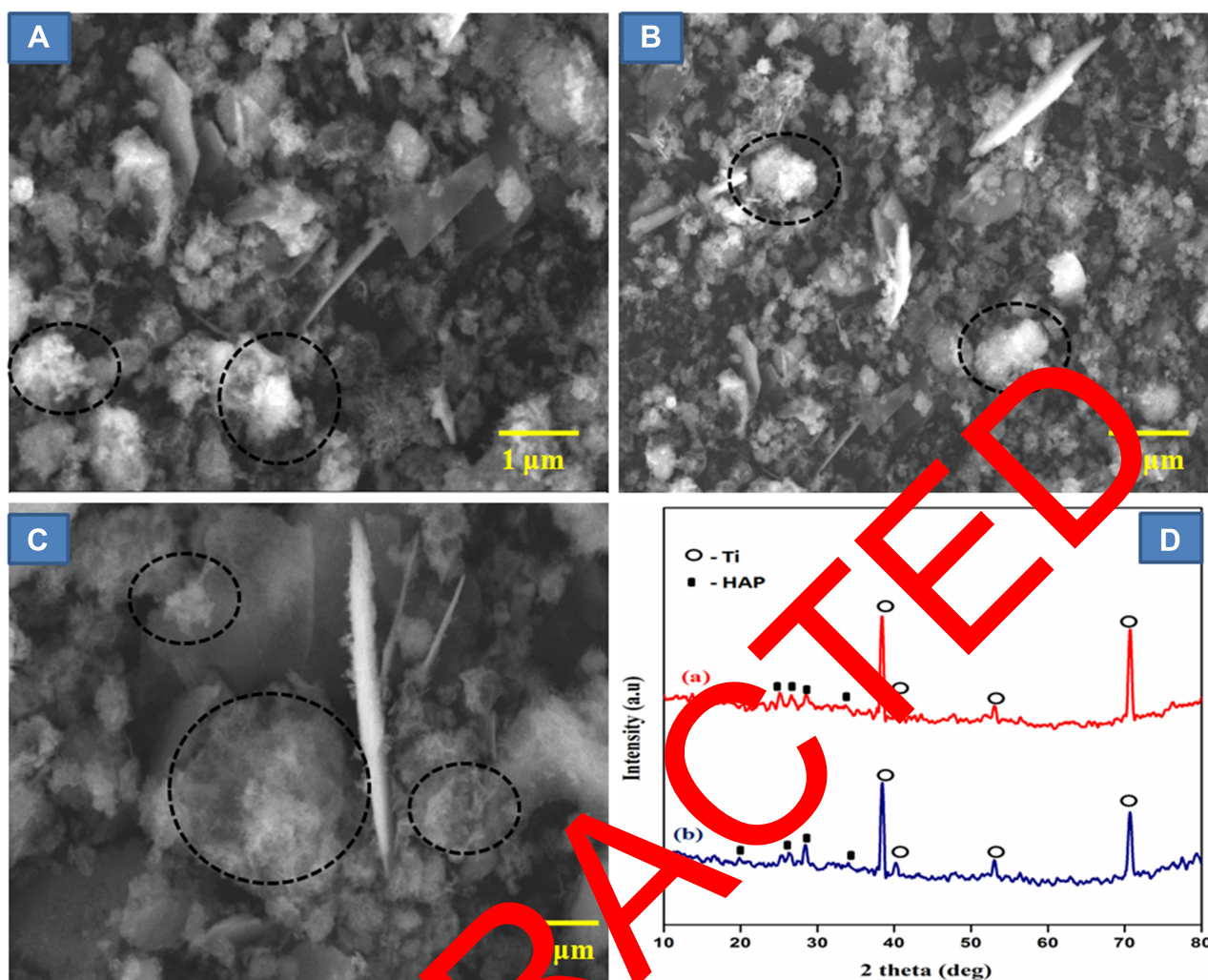
Figure 9 Formation of apatite crystals on the surface of MHAP/AV composite-coated PD-Ti plate after immersion in SBF for (**A**) 1 day, (**B**) 3 days and (**C**) 7 days. The formation of apatite crystals over the rod morphology is indicated in a black circle. (**D**) XRD spectra of MHAP/AV composite-coated PD-Ti plate after immersion in SBF for (a) 1 day and (b) 7 days.

intense peak at 2θ ~ 28° becomes more intense at the 7th day of immersion, as shown in Figure 9Db. Moreover, the peaks near 26° in both of the diffraction patterns reveal the formation of apatite on the surface of the immersed Ti plate. The decreasing intensity of the Ti peak at 40° and an increase of HAP peak at 28° in Figure 9Db show the apatite structure was significantly formed on the surface of the Ti plate.

Evaluation of Mechanical Strength by Vickers Micro-Hardness Analysis

In orthopedic bone implantation, the mechanical strength of an implant has been considered as a potential factor in predicting the strength of the implants for avoiding the implant failure during insertion into the body. In the case of load-

bearing applications, under pressure created by the body, the perfect implant is to be designed for withstanding that pressure. Our previous study reveals that the pure surface-treated Ti plate has a micro-hardness value of 829.7 ± 14.95.[46] Nelson Elias et al in 2019,[56] were proved the concept that surface treatment of commercially pure Ti will increase the hardness value, and due to this increment, the material becomes more reliable, and it can reduce the chance of deformation during implantation. In this study, the micro-hardness of the PD-Ti plates (with and without the MHAP/AV composite coating) was investigated, and the results are given in Table 1. Initially, the PD-Ti plate exhibits the micro-hardness of 188.9 ± 2.91 Hv, and for MHAP/AV-coated PD-Ti exhibits 200.1 ± 2.29 Hv. When compared these results with pure Ti (829.7 ± 14.95), the obtained micro-hardness was decreased. But it is appropriate for implantation on the

Table 1 Micro-Hardness Values of All Triplicated Experiments with the Maximum, Minimum and Mean Values of PD-Treated Ti and MHAP/AV-Coated PD-Ti Plates

PD-Ti Plate		MHAP/AV-Coated PD-Ti Plate	
Test No	Hardness (Hv)	Test No	Hardness (Hv)
1	191.20	1	198.42
2	186.61	2	198.42
3	188.89	3	203.46
Max	191.20	Max	203.46
Min	186.61	Min	198.42
Mean	188.90	Mean	200.10

rat model. In 2009, Sun et al[57] reported for the applications of astronauts had measured the hardness value of the femur bone of rats, and they find out the effect of microgravity on the bone skeleton by the nano-indentation method. They estimated the hardness value of the normal rats as 0.49 ± 0.16 GPa (49.0 Hv). By comparing the hardness value with the normal femur bone of rat, the MHAP/AV-coated PD-Ti implant has a higher micro-hardness value due to the MHAP/AV coating. This coating will much resist to plastic deformation of the implant material when embedded in the body. So it will not undergo any failure during in-vivo implantation.

Biological Analysis
In-vitro Analysis of Synthesized Compounds
MG-63 Osteoblasts Cells Proliferation, Morphology and ALP Activity

MG-63 osteoblasts-like cells were here taken to evaluate the bio-compatibility of the fabricated HAP, MHAP, HAP/AV and MHAP/AV composites. HAP was taken as reference in all the period of investigation. Interestingly, 1st day of the treatment of MG-63 cells with different testing samples (HAP, MHAP, HAP/AV and MHAP/AV), the viability was not affected. The feasibility of cells on various materials for 1st day was the same as the viability of HAP (control) on 1st day of treatment. On the 3rd day of incubation, the viability was decreased in all testing samples. However, further increases in the treatment period, the growth of cells was also increased simultaneously for 7th and 14th days of incubation with various testing samples, and it reached the maximum (90%) for 14th day with MHAP/AV composite as showed in Figure 10A. The optical microscopy images of the viability of cells are given in Figure 11, which is also evidence for the effect of different testing samples on MG-63 osteoblasts cells

for various treatment times such as 1, 3, 7 and 14 days (Figure 11 (A–D) for HAP, (E–H) for MHAP, (I–L) for HAP/AV and (M–P) for MHAP/AV). These results are due to the combined impact of lanthanide trivalent minerals and the AV compound that are present in the MHAP/AV composite, which stimulates osteoblast activity by the sustained and prolongs effects. Thereby conclude, the substitution of minerals and an external organic moiety (AV) on HAP did significantly influence the viability of MG-63 osteoblasts cells, as reported by our group previously.[46]

ALP is an essential marker for osteoblast differentiation since ALP is considered as; it plays a crucial role in initiating the Ca^{2+} mineralization by cell differentiation. As a result of the calcification process, the concentration of phosphatase being increases as the stimulation of osteoblasts differentiation. The ALP activities of MG-63 osteoblast cells on different testing samples on different treatment periods are shown in Figure 10. In all groups of samples, the ALP activity was increased as the increases of the period of treatment, and it attains maximum at the 14th day of treatment with MHAP/AV composite, as shown in cell viability studies because of the presence of lanthanide ions and AV compounds collectively. That could be explained the osteoconductive nature of the MHAP/AV composite facilitates higher ALP production. The activity at 14th day was significantly higher than that of 1st day of treatment in all groups, including control groups (HAP). In both cell viability and ALP studies, at all periods except day 1, the MHAP/AV composite showed significantly higher cell viability and ALP activity on MG-63 cells when compared with pure HAP control.

Qualification and Quantification of Mineralization by ARS Staining

Evaluation of an inorganic Ca^{2+} ion on the cell surface is evident for the bone-like apatite structure formation. The calcium mineralization by cells would be a help to the osteoblast cell production and differentiation. When the osteoblast cells were treated with ARS stain, it will bind with inorganic Ca^{2+} ion that presents in the mineralized extracellular matrix (ECM) of the osteoblast cell's surface that produces the intense red stains over the surface of the osteoblasts cells. As shown in Figure 12, all the groups experience different trends under different conditions for periods of treatment such as 1, 3, 7, and 14 days (Figure 12 (A–D) for HAP, (E–H) for MHAP, (I–L) for HAP/AV and (M–P) for MHAP/AV). It was clear that the bright red color intensity was maximum at 7 days (Figure 12C and G and K and O) and 14 days (Figure 12D and H and L and
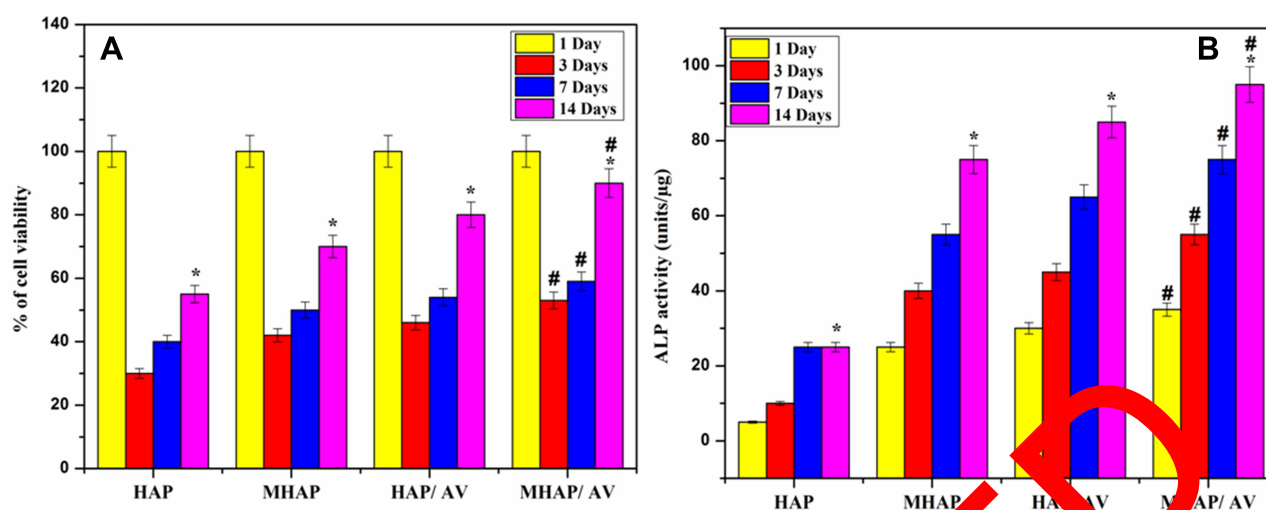
Figure 10 MG-63 osteoblast cells proliferation evaluated by MTT assay (**A**) and ALP activity of the MG-63 osteoblast cells (**B**) on different testing samples. *Comparison of the denoted group with the same set at 1 day of treatment time *p < 0.05. #Comparison of the denoted group with the HAP control at the same time period #p < 0.05.
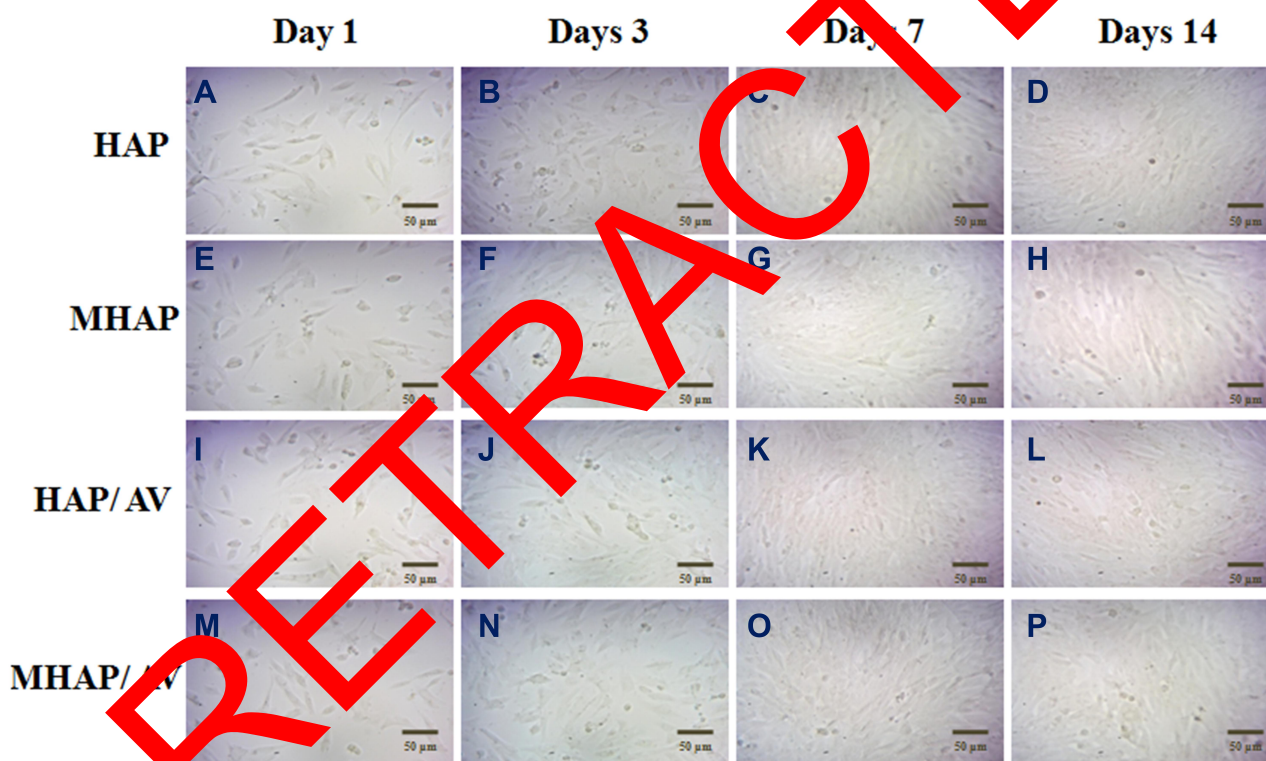

Figure 11 Optical microscopy images of MG-63 osteoblast cells after treated with HAP (**A–D**), MHAP (**E–H**), HAP/AV (**I–L**) and MHAP/AV (**M–P**) for different time days such as 1, 3, 7 and 14 days.

P) when compared with other treatment periods such as 1 day (Figure 12A and E and I and M) and 3 days (Figure 12B and F and J and N) of treatment. The smaller and moderate intensity of red color was shown in 1 day and 3 days, respectively. In all groups, compared to the 14th day of treatment, the staining after the 7th day of culture showed less intense red stain. Even

though the HAP/AV composite has shown bright, intense red stain at the 14th day of staining, obvious the enhancement in Ca^{2+} mineralization and results more positive effects. The maximum bright red colored stain was observed on the MHAP/AV treated cells and the result explains the MHAP/AV composite is more beneficial for bone regeneration by
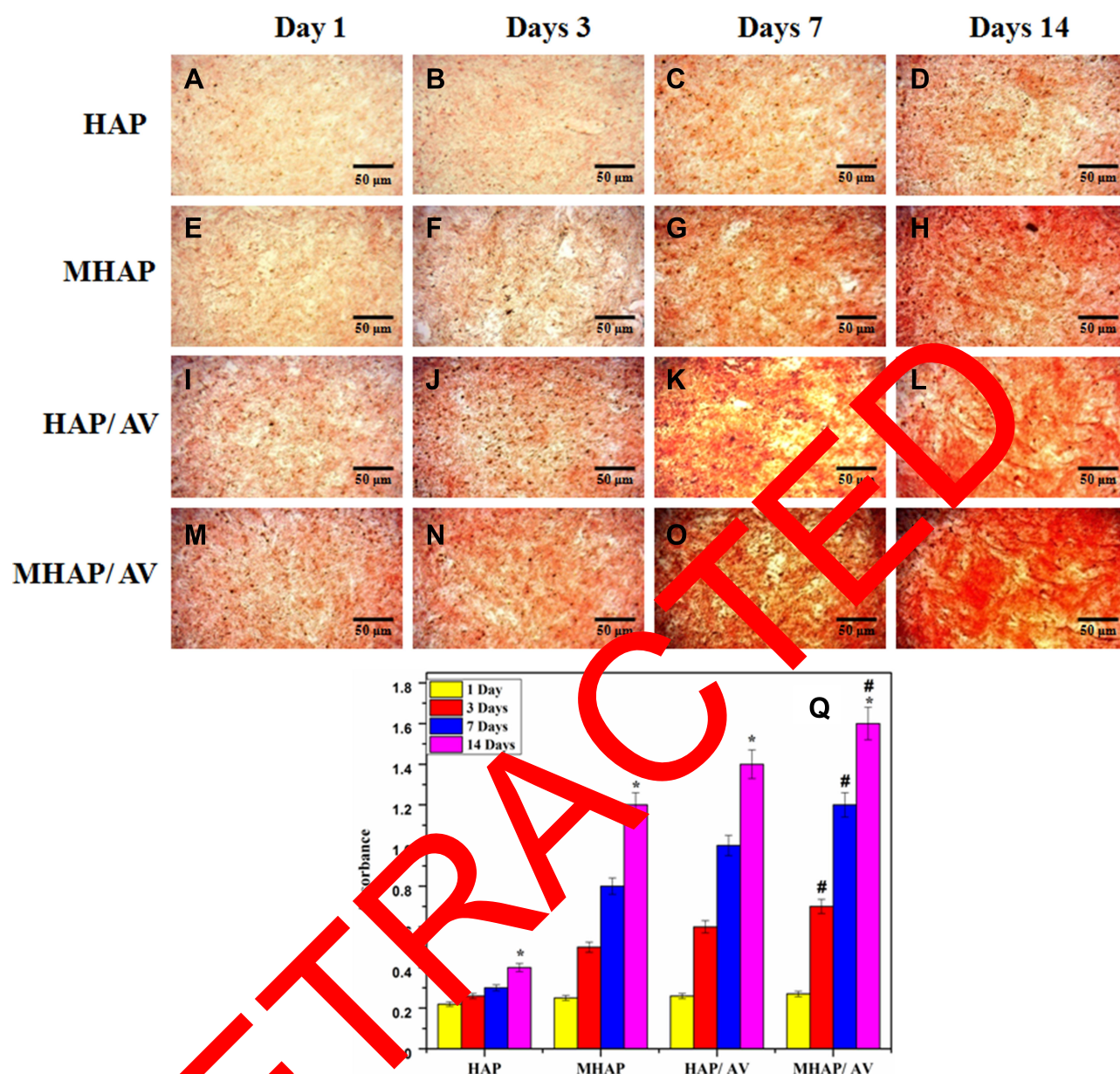
Figure 12 Mineralization ARS staining of MG-63 osteoblast cells cultured on HAP (**A–D**), MHAP (**E–H**), HAP/AV (**I–L**), and MHAP/AV (**M–P**) for 1, 3, 7 and 14 days. (**Q**) Quantification of deposition of minerals.*Comparison of the denoted group with the same set at 1st day of treatment time *p < 0.05. #Comparison of the denoted group with the HAP control at the same time period #p < 0.05.

enabling osteoblasts proliferation, differentiation, and inorganic apatite deposition. Besides the microscopic evaluations, the calcium quantification by ARS stained cells with 10% CPC was performed. As shown in Figure 12Q, the MG-63 osteoblast cells exhibit more calcium content in the 14th day of treatment period than other periods. Similar passion was continued in different groups of compounds also. Like time variation, the calcium deposition was also varied depends upon the composites treated. At the 14th day of treatment with MHAP/AV composite, the calcium content was significantly higher

than other groups (Figure 12Q). As ALP and ARS results, the calcium mineralization also exhibits significantly higher positive effects against osteoblasts-like cells by the composite MHAP/AV without showing any cytotoxicity when compared with pure HAP control.

In-vivo Animal Studies
Histological Studies for New Bone-Cell Formation
From the better results of in-vitro analysis by the prepared composites, the in-vivo osteogenic ability of the MHAP/AV

composite coated on PD-Ti material was assessed in 4 weeks of implantation. The MHAP/AV composite exhibit the better bio-compatibility and osteogenic activity against MG-63 cells. From these in-vitro results, we had further chosen this composite for coating in the PD-Ti plate for in-vivo implantation on a rat model for tibia defect repair. This is the primary indicator of the osteogenic ability of the fabricated implant for orthopedic applications. Figure 13 represents the corresponding staining images at 1st, 2nd, 3rd and 4th week of implantation to confirm the reconstruction of defected bone by MHAP/AV-coated PD-Ti implant. Figure 13B–E corresponds to the images of implanted tissues stained by MT staining. The more support from MT staining was observed in terms of more deposition of collagen protein, and it was indicated by blue color. This collagen protein deposition was fewer at 1st week of implantation, where only the connecting tissues appeared. At the 2nd and 3rd week, the more collagen protein was observed with the presence of connecting tissues. The change of staining color from blue to red indicates the formation of new bone tissues at the 4th week of implantation.[58,59] From these results, it was concluded that the implant has good bio-compatible nature, and it induces the connecting tissue formation on the bone defect.

Figure 13G–J represents the images of HE staining of the retrieved implanted tissue. This clearly demonstrates the implant with the MHAP/AV coated on the PD-Ti plate was successfully facilitated the growth of new bone tissue at the 4th week of implantation evident from the visible of more red staining along with scattered osteoblasts. Initial periods of implantation, the presence of osteoblasts was stained by blue color (indicated by the red arrow). These osteoblasts will further develop the new bone via the osteoids formation

(indicated by the blue arrow). During the osteoblast differentiations into new bone formation, the osteoids are embedded in that newly formed bone tissue, as shown at the 4th week of implantation (Figure 13J). Thus the bone reconstruction process actively progressed in MHAP/AV composite coated on PD-Ti implant after 4th week of the implant through the osteogenic differentiation.[60] In both of the MT and HE staining, the tissue of an un-defected rat was used as a control as shown in Figure 13A and F

X-Ray Radiograph Analysis

As shown in the area under the dotted circle of the X-Ray image in Figure 14A, the critical-sized tibia bone defect was made by mechanical drilling. After creating a defect, it was filled by an implant made by MHAP/AV coated on the PD-Ti plate. The MHAP/AV composite could well adjust the uneven bone defect in order to heal the defect by the allowing to the proliferation of osteoblast cells on the entire Ti implant at 4th week of implantation as evidenced from Figure 14B, where it was clearly seen the new bone cells were infiltrated into the defect site. From these results, the MHAP/AV composite could have a positive effect on the tibia bone defect. Moreover, the treating of the surface of the Ti implant by PD had not exhibited any unpredictable impact. This treating of the Ti surface with PD and MHAP/AV composite has more advantages to increasing osteoblast cell proliferation and differentiation.

Present results were correlated with our previous study[46] where the new bone formation was being started after the first week by the formation of osteoblast cells and osteoids. The matured bone formation was fully covered the defect site at 4th week of implantation as showed by this work and similar
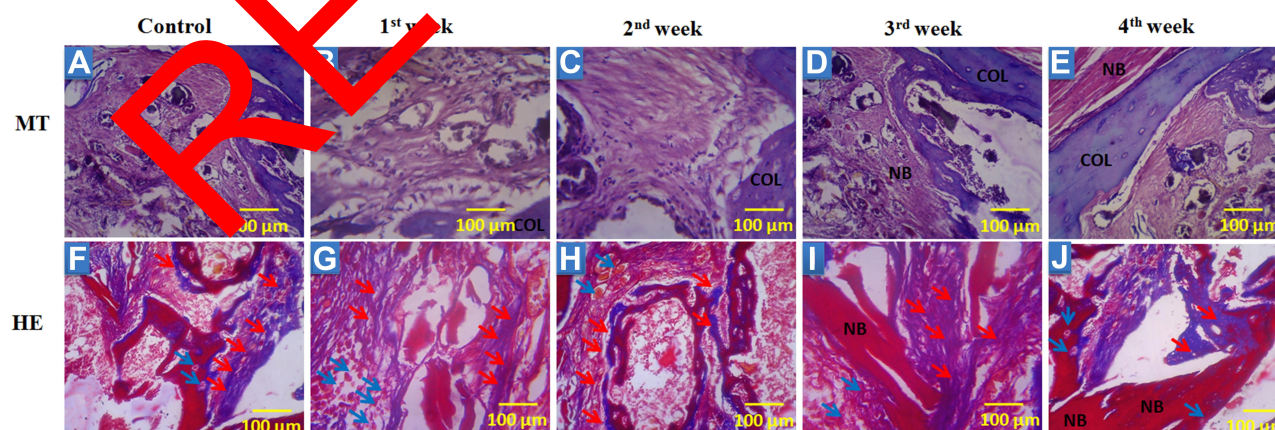

Figure 13 Representative MT (**A–E**) and HE staining (**F–J**) of retrieved implant section at 1st, 2nd, 3rd, and 4th week of surgical experiment with MHAP/AV coated on PD-Ti implant. Red arrow indicates Osteoblasts; Blue arrow indicates Osteoids.
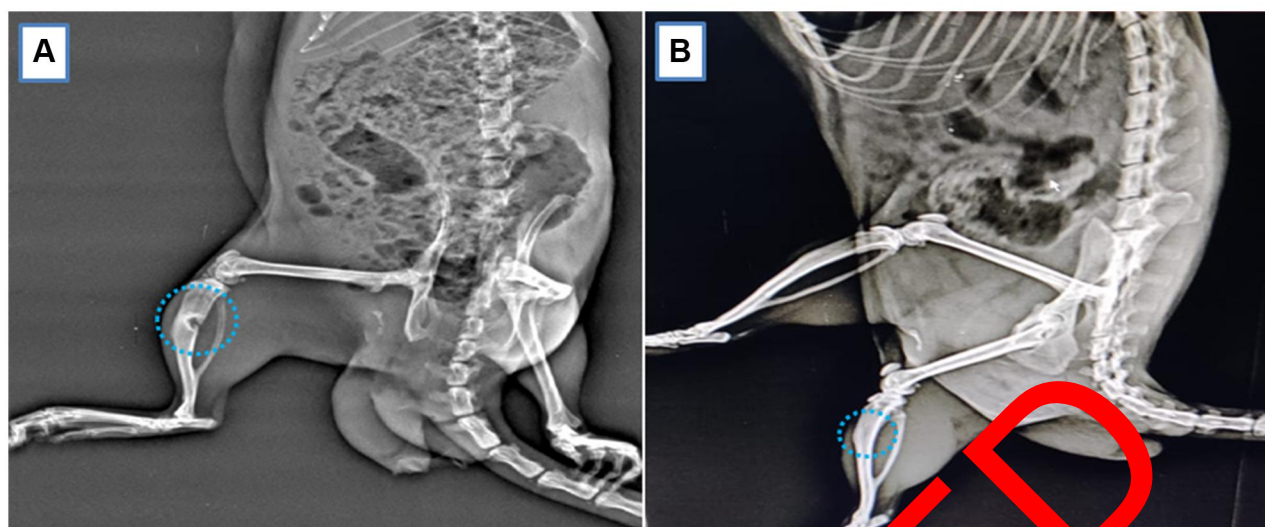**Abbreviations**: COL, collagen; NB, new bone.

Figure 14 X-ray images of (**A**) defected rat and (**B**) 28th day of treatment with MHAP/AV-coated PD-Ti plate implantation.

result was evaluated by Yin et al, in 2020.[61] They have treated the tibia bone defect with the calcium alginate reinforced MHAP/poly (vinyl pyrrolidone) composite-coated Ti plate. Another study was performed by Banerjee and Bose in 2019 by the surface of Ti implant with natural AV gel extract; acemannan incorporated Ag and Si-doped HAP.[31] The in-vivo new bone formation was identified after 5 weeks of implantation. By comparing our results with previously reported literature, it was known that our fabricated implant material would also serve as better bio-material to load bearing hard tissue regeneration in the orthopedic field.

Conclusions

In this work, the natural bioactive extract derived from AV leaf was successfully reinforced with the lanthanides (La, Ce, and Gd)-substituted HAP matrix. The mechanical strength revealed that the microhardness of the Ti plate is higher in MHAP/AV-coated PD-Ti than uncoated PD-Ti. In-vitro experiments such as MG-63 osteoblast cell proliferation, differentiation and calcium deposition reveal that the prepared MHAP/AV composite shows more bio-active osteogenic potential among other groups such as HAP, MHAP, and HAP/AV composite. It could explain by the synergetic osteogenic ability of all lanthanide ions and organic AV compounds in MHAP/AV composite. The same effect was reflected in the in-vivo investigation also. The surface treatment of Ti plate with PD was enhancing the coating characterization, and also it did not produce any cytotoxicity on a rat model. Therefore, our work demonstrates that the natural AV compound is good for orthopedic application when combined with HAP matrix.

Moreover, the lanthanide trivalent ions also induce osteoblast proliferation and help for bone regeneration. Besides, the higher affinity of PD towards bio-molecules containing thiols or primary amines, our fabricated PD-treated implant, can also serve as a drug carrier for drug delivery applications in osteosarcoma tissue engineering in the future.

Abbreviations

ALP, alkaline phosphatase; ARS, Alizarin Red staining; AV, *Aloe vera*; Ca, calcium; Ce, cerium; cp Ti, commercially pure titanium; EPD, electrophoretic deposition; FT-IR, Fourier-transform infrared microscope; Gd, gadolinium; HAP, hydroxyapatite; HE, hematoxylin and eosin; HR-TEM, high-resolution transmission electron microscope; La, lanthanum; MT, Masson's trichrome; MTT, 3-(4,5-dimethyl-2-thiazolyl)-2,5-diphenyl-2H-tetrazolium bromide; P, phosphate; PD, polydopamine; SEM, scanning electron microscope; XRD, x-ray diffractometer.

Disclosure

The authors report no conflicts of interest in this work.

References

1. Li Y, Yang C, Zhao H, Qu S, Li X, Li Y. New developments of Ti-based alloys for biomedical applications. *Materials*. 2014;7:1709–1800. doi:10.3390/ma7031709

2. Alvarez K, Nakajima H. Metallic scaffolds for bone regeneration. *Materials*. 2009;2:790–832. doi:10.3390/ma2030790

3. Karbowniczek J, Muhaffel F, Cempura G, Cimenoglu H, Czyrska-Filemonowicz A. Influence of electrolyte composition on microstructure, adhesion and bioactivity of micro-arc oxidation coatings produced on biomedical Ti6Al7Nb alloy. *Sur Coat Tech*. 2017;321:97–107. doi:10.1016/j.surfcoat.2017.04.031

4. Hao J, Li Y, Wang X, et al. Corrosion resistance and biological properties of a micro–nano structured Ti surface consisting of TiO2 and hydroxyapatite. *RSC Adv*. 2017;7:33285–33292. doi:10.1039/c7ra01175j

5. Shamray VF, Sirotinkin VP, Smirnov IV, et al. Structure of the hydroxyapatite plasma-sprayed coatings deposited on pre-heated Titanium substrates. *Cer Int*. 2017;43:9105–9109. doi:10.1016/j.ceramint.2017.04.057

6. Kumari R, Duttamajumdar J. Wear behavior of plasma spray deposited and post heat-treated hydroxyapatite (HA)-based composite coating on titanium alloy (Ti-6Al-4V) substrate. *Metal Mat Trans A*. 2018;7. doi:10.1007/s11661-018-4626-z

7. Lini Z, Li SJ, Sun F, Ba DC, Li XC. Surface characteristics of a dental implant modified by low energy oxygen ion implantation. *Sur Coat Tech*. 2018;365:208–213. doi:10.1016/j.surfcoat.2018.09.003

8. Shanaghia A, Chu PK. Enhancement of mechanical properties and corrosion resistance of NiTi alloy by carbon plasma immersion ion implantation. *Sur Coat Tech*. 2018;365:52–57. doi:10.1016/j.surfcoat.2018.04.027

9. Wang H, Chen T, Cong W, Liu D. Laser cladding of Ti-based ceramic coatings on Ti6Al4V alloy: effects of CeO2 nanoparticles additive on wear performance. *Coatings*. 2019;9:1–17. doi:10.3390/coatings9020109

10. Shinonaga T, Tsukamoto M, Kawa T, Chen P, Nagai A, Hanawa T. Formation of periodic nanostructures using a femto second laser to control cell spreading on titanium. *Appl Phys B*. 2015;119. doi:10.1007/s00340-015-6082-4

11. Wang L, Xie L, Lv Y, et al. Microstructure evolution and super elastic behavior in Ti-35Nb-2Ta-3Zr alloy processed by friction stir processing. *Act Mat*. 2017;131:499–510. doi:10.1016/j.actamat.2017.03.079

12. Gu H, Ding Z, Yang Z, et al. Microstructure evolution and electro-chemical properties of TiO2/Ti-35Nb-2Ta-3Zr micro/nano-composites fabricated by friction stir processing. *Mat.Des*. 2019;169:107680. doi:10.1016/j.matdes.2019.107680

13. Silverman HG, Roberto FF. Understanding marine mussel adhesion. *Springer Science Business Media*. 2007;9:661–681. doi:10.1007/s10126-007-9053-x

14. Herbert Waite J. Adhesion a` la Moule. *Integr Comp Biol*. 2002;42:1172–1180. doi:10.1093/icb/42.6.1172

15. Tejido-Rastrilla R, Ferraris S, Goldmann WH, et al. Studies on cell compatibility, antibacterial behavior, and zeta potential of Ag-containing polydopamine-coated bioactive glass-ceramic. *Materials*. 2019;12:500. doi:10.3390/ma12030500

16. Ku SH, Lee JS, Park CB. Spatial control of cell adhesion and patterning through mussel-inspired surface modification by polydopamine. *Langmuir*. 2010;26:15104–15108. doi:10.1021/la102825p

17. Ye Q, Zhou F, Liu W. Bioinspired catecholic chemistry for surface modification. *Chem Soc Rev*. 2011;40:4244–4258. doi:10.1039/c1cs15026j

18. Lee H, Dellatore SM, Miller WM, Messersmith PB. Mussel-inspired surface chemistry for multifunctional coatings. *Science*. 2007;318:426–430. doi:10.1126/science.1147241

19. Jia J, Han F, Wang H, et al. Polydopamine-assisted surface modification for orthopedic implants. *J Ortho Trans*. 2019;17:82–95. doi:10.1016/j.jot.2019.04.001

20. Wang Z, Li P, Jiang Y, et al. Mussel-inspired nano structured coatings assembled using polydopamine nanoparticles and hydroxyapatite nanorods for biomedical applications. *Bio Biot*. 2017;3:1–10. doi:10.1016/j.bsbt.2017.01.001

21. Khetani S, Yong KW, Ozhukil Kollath V, et al. Engineering shelf-stable coating for microfluidic organ-on-a-chip using bioinspired catecholamine polymers. *ACS Appl Mater Interfaces*. 2020;12:6910–6923. doi:10.1021/acsami.9b20826

22. Khetani S, Yong KW, Guan K, et al. UV-triggered polymerization of polycatecholamines enables the production of organ-on-chips inside a biosafety cabinet. *App Mat Tod*. 2020;20:100721. doi:10.1016/j.apmt.2020.100721

23. Surjushe A, Vasani R, Saple DG. Aloe vera: a short review. *Indian J Dermatol*. 2008;53:163–166. doi:10.4103/0019-5154.44785

24. Jasso de Rodr´ıguez D, Hernández-Castillo D, Rodr´ıguez-Garc´ıa R, Angulo-Sánchez JL. Antifungal activity in vitro of aloe vera pulp and liquid fraction against plant pathogenic fungi. *Inds Cro Prod*. 2005;21:81–87. doi:10.1016/j.indcrop.2004.01.002

25. Athiban PP, JyotiBorthakur B, Ganesan SB. Evaluation of antimicrobial efficacy of aloe vera and its effectiveness in decontaminating gutta percha cones. *J Cons Den*. 2012;15:246–248. doi:10.4103/0972-0707.97949

26. Hu Y, Xu J, Hu Q. Evaluation of antioxidant potential of aloe vera (Aloe barbadensis Miller) extracts. *J Agric Food Chem*. 2003;51:7788–7791. doi:10.1021/jf034255i

27. Agnes Mary S, Giri Dev VR. Electrospun herbal nanofibrous wound dressings for skin tissue engineering. *J Tex Ins*. 2015;106:886–895. doi:10.1080/00405000.2014.951247

28. Suganya S, Venugopal J, Agnes Mary S, Ramakrishna S, Lakshmi BS, GiriDev VR. Aloe vera incorporated biomimetic nanofibrous scaffold: a regenerative approach for skin tissue engineering. *Iran Polym J*. 2014;23:237–248. doi:10.1007/s13726-013-0219-2

29. Rahman S, Carter P, Bhattarai N. Aloe vera for tissue engineering applications. *J Funct Biomater*. 2017;8:1–17. doi:10.3390/jfb8010006

30. Jithendra P, Merlin Rajam A, Kalaivani T, Baran Mandal A, Rose C. Preparation and characterization of aloe vera blended collagen chitosan composite scaffold for tissue engineering applications. *ACS Appl Mater Interfaces*. 2013;5:7291–7298. doi:10.1021/am401637c

31. Suganya S, Venugopal JR, Ramakrishna S, Lakshmi BS, Giridev VR. Aloe vera/silk fibroin/hydroxyapatite incorporated electrospun nanofibrous scaffold for enhanced osteogenesis. *J Biomim Biomat Tis Eng*. 2014;4(1):9–19. doi:10.1166/jbt.2014.1139

32. Banerjee D, Bose S. Effects of aloe vera gel extract in doped hydroxyapatite-coated titanium implants on in vivo and in vitro biological properties. *ACS Appl Bio Mater*. 2019;8:3194–3202. doi:10.1021/acsabm.9b00077

33. Panichev AM. Rare Earth elements: review of medical and biological properties and their abundance in the rock materials and mineralized spring waters in the context of animal and human geophagia reasons evaluation. *Ach Life Sci*. 2015;9:95–103. doi:10.1016/j.als.2015.12.001

34. Zhou H, Lee J. Nanoscale hydroxyapatite particles for bone tissue engineering. *Act Biomat*. 2011;7:2769–2781. doi:10.1016/j.actbio.2011.03.019

35. Martins MA, Santos C, Margarida Almeida M, Costa MEV. Hydroxyapatite micro- and nanoparticles: nucleation and growth mechanisms in the presence of citrate species. *J Col Int Sci*. 2008;318:210–216. doi:10.1016/j.jcis.2007.10.008

36. Lou W, Dong Y, Zhang H, et al. Preparation and characterization of lanthanum-incorporated hydroxyapatite coatings on titanium substrates. *Int J Mol Sci*. 2015;16:21070–21086. doi:10.3390/ijms160921070

37. Shah V, Shah S, Shah H, et al. Antibacterial activity of polymer coated cerium oxide nanoparticles. *PLoS One*. 2012;7:e47827. doi:10.1371/journal.pone.0047827

38. Albuquerque Passos Farias I, Christiano Lima Dos Santos C, CorreiaSampaio F. Antimicrobial activity of cerium oxide nanoparticles on opportunistic microorganisms: a systematic review. *Bio Med Res Inter*. 2018;1–14. doi:10.1155/2018/1923606

39. Zhu DY, Lu B, Yin J-H, et al. Gadolinium-doped bioglass scaffolds promote osteogenic differentiation of hBMSC via the Akt/GSK3β pathway and facilitate bone repair in vivo. *Int J Nanomed*. 2019;17:1085–1100. doi:10.2147/IJN.S193576

40. Wang L, Shang X, Hao Y, et al. Bi-functional titanium-polydopamine-zinc coatings for infection inhibition and enhanced osseointegration. *RSC Adv*. 2019;9:2892–2905. doi:10.1039/c8ra09112a

41. Kokubo T, Takadama H. How useful is SBF in predicting in vivo bone bioactivity? *Bio Mat*. 2006;27:2907–2915. doi:10.1016/j.biomaterials.2006.01.017

42. Sumathra M, Kumar Sadasivuni K, Suresh Kumar S, Rajan M. Cisplatin-loaded graphene oxide/chitosan/hydroxyapatite composite as a promising tool for osteosarcoma-affected bone regeneration. *ACS Omega*. 2018;3:14620–14633. doi:10.1021/acsomega.8b02090

43. Shalumon KT, JyunLai G, Hao Chen C, Ping Chen J. Modulation of bone-specific tissue regeneration by incorporating bone morphogenetic protein and controlling the shell thickness of silk fibroin/chitosan/nano-hydroxyapatite core−shell nanofibrous membranes. *ACS Appl Mater Interfaces*. 2015;7:21170–21181. doi:10.1021/acsami.5b04962

44. Gao X, Song J, Zhang Y, et al. Bioinspired design of polycaprolactone composite nanofibers as artificial bone extracellular matrix for bone regeneration application. *ACS Appl Mater Interfaces*. 2016;8:27594–27610. doi:10.1021/acsami.6b10417

45. Govindaraj D, Rajan M, Munusamy MA, Alarfaj AA, Kumar Sadasivuni K, Suresh Kumar S. The synthesis, characterization and in vivo study of mineral substituted hydroxyapatite for prospective bone tissue rejuvenation applications. *Nanomed Nanotech Bio Med*. 2017;13:2661–2669. doi:10.1016/j.nano.2017.07.017

46. Pan J, Prabakaran S, Rajan M. In-vivo assessment of minerals substituted hydroxyapatite/poly sorbitol sebacate glutamate (PSSG) composite coating on titanium metal implant for orthopedic implantation. *Biomed Pharma*. 2019;119:109404. doi:10.1016/j.biopha.2019.109404

47. Gabriela C, Ana Maria B, Constantin I. New Tin (IV)-substituted hydroxyapatite nanoparticles: preparation and characterization. *Ceram Inter*. 2015;41:12192–12201. doi:10.1016/j.ceramint.2015.06.040

48. Luo H, Xie J, Xiong L, et al. Engineering photoluminescent and magnetic lamellar hydroxyapatite by facile one-step Se/Gd dual-doping. *J Mater Chem B*. 2018;6:3515–3521. doi:10.1039/C8TB00658J

49. Xi Lim Z, Yew Cheong K. Effects of drying temperature and ethanol concentration on bipolar switching characteristics of natural aloe vera-based memory devices. *Phys Chem Chem Phys*. 2015;17:26833–26853. doi:10.1039/c5cp04622j

50. Swami Hulle NR, Patruni K, Srinivasarao P. Rheological properties of aloe vera (aloebarbadensis miller) juice concentrates. *J Food Pro Eng*. 2014;37:375–386. doi:10.1111/jfpe.12093

51. Alexopoulou M, Mystiridou E, Mouzakis D, et al. Preparation, characterization and in vitro assessment of ibuprofen loaded calcium phosphate/gypsum bone cements. *Cryst Res Technol*. 2015;1:41–48. doi:10.1002/crat.201500143

52. Selvakumar M, Kumar Jaganathan S, Nando G, Chattopadhyay S. Synthesis and characterization of novel polycarbonate based polyurethane/polymer wrapped hydroxyapatite nanocomposites: mechanical properties, osteoconductivity and biocompatibility. *J Biomed Nanotech*. 2015;11:291–305. doi:10.1166/jbn.2015.1975

53. Zhang H, Li S, Ma X, Yang D. Controllable growth of dendrite-like CuO nanostructures by ethylene glycol assisted hydrothermal process. *Mat Res Bull*. 2008;1296. doi:10.1016/j.materresbull.2007.05.017

54. Li Y, Jing Z, Xiaoming S, Zhixiang D, Yadong L. Formation of rod-like Mg(OH)2 nanocrystallite under hydrothermal conditions and the conversion to MgO nanorod by thermal dehydration. *Mat Che Phy*. 2002;76:119–122. doi:10.1016/S0254-0584(01)00509-0

55. Botelho CM, Lopes MA, Gibson IR, Best SM, Santos JD. Structural analysis of Si-substituted hydroxyapatite: zeta potential and X-ray photoelectron spectroscopy. *J Mat Sci Mat Med*. 2002;13:1123–1127. doi:10.1023/A:1021176012888

56. Nelson Elias C, Mogaib Fernandes D, Moura de Souza F, Dos Santos Monteiro E, Sérgio de Biasi R. Mechanical and clinical properties of titanium and titanium-based alloys (Ti G2, Ti G4 cold worked nanostructured and Ti G5) for biomedical applications. *J Mater Res Technol*. 2019;8:1060–1069. doi:10.1016/j.jmrt.2018.07.016

57. Sun LW, Fan YB, Li DY, et al. Evaluation of the mechanical properties of rat bone under simulated microgravity using nanoindentation. *Acta Bio*. 2009;5:3506–3511. doi:10.1016/j.actbio.2009.04.042

58. Song JE, Tripathy N, Shin JH, et al. In vivo bone regeneration evaluation of duck's feet collagen/PLGA scaffolds in rat calvarial defect. *Mol Res*. 2017;25:994–999. doi:10.1007/s13233-017-5134-5

59. Dhivya S, Keshav Narayan A, Logith Kumar R, Viji Chandran S, Vairamani M, Selvamurugan N. Proliferation and differentiation of mesenchymal stem cells on scaffolds containing chitosan, calcium polyphosphate and pigeonite for bone tissue engineering. *Cell Proli*. 2018;51:e12408. doi:10.1111/cpr.12408

60. Duan B, Shou K, Su X, et al. Hierarchical microspheres constructed from chitin nanofibers penetrated hydroxyapatite crystals for bone regeneration. *Bio Macro*. 2017;18:2080–2089. doi:10.1021/acs.biomac.7b00408

61. Yin X, Yan L, Hao DJ, et al. Calcium alginate template-mineral substituted hydroxyapatite hydrogel coated titanium implant for tibia bone regeneration. *Inter J Pharm*. 2020;582:119303. doi:10.1016/j.ijpharm.2020.119303

RETRACTED